Remote Sensing of Environment 251 (2020) 112062

Contents lists available at ScienceDirect

Remote Sensing of Environment

journal homepage: www.elsevier.com/locate/rse

Synergistic use of SMAP and OCO-2 data in assessing the responses of ecosystem productivity to the 2018 U.S. drought

Xing Li[a], Jingfeng Xiao[a,*], John S. Kimball[b], Rolf H. Reichle[c], Russell L. Scott[d], Marcy E. Litvak[e], Gil Bohrer[f], Christian Frankenberg[g,h]

[a] Earth Systems Research Center, Institute for the Study of Earth, Oceans, and Space, University of New Hampshire, Durham, NH 03824, USA
[b] Numerical Terradynamic Simulation Group, College of Forestry & Conservation, University of Montana, Missoula, MT, USA
[c] Global Modeling and Assimilation Office, NASA Goddard Space Flight Center, Greenbelt, MD 20771, USA
[d] Southwest Watershed Research Center, USDA-ARS, Tucson, AZ 85719, USA
[e] Department of Biology, University of New Mexico, Albuquerque, NM 87131, USA
[f] Department of Civil, Environmental and Geodetic Engineering, Ohio State University, Columbus, OH 43210, USA
[g] Division of Geological and Planetary Sciences, California Institute of Technology, Pasadena, CA 91125, USA
[h] Jet Propulsion Laboratory, California Institute of Technology, Pasadena, CA 91109, USA

ARTICLE INFO

Keywords:
Soil Moisture Active Passive
Orbiting Carbon Observatory-2
GOSIF
Soil moisture
Sun-induced chlorophyll fluorescence
Gross primary production
Water stress
Dryland
Carbon cycle
Crop yield
Enhanced vegetation index

ABSTRACT

Soil moisture and gross primary productivity (GPP) estimates from the Soil Moisture Active Passive (SMAP) and solar-induced chlorophyll fluorescence (SIF) from the Orbiting Carbon Observatory-2 (OCO-2) provide new opportunities for understanding the relationship between soil moisture and terrestrial photosynthesis over large regions. Here we explored the potential of the synergistic use of SMAP and OCO-2 based data for monitoring the responses of ecosystem productivity to drought. We used complementary observational information on root-zone soil moisture and GPP (9 km) from SMAP and fine-resolution SIF (0.05°; GOSIF) derived from OCO-2 SIF soundings. We compared the spatial pattern and temporal evolution of anomalies of these variables over the conterminous U.S. during the 2018 drought, and examined to what extent they could characterize the drought-induced variations of flux tower GPP and crop yield data. Our results showed that SMAP GPP and GOSIF, both freely available online, could well capture the spatial extent and dynamics of the impacts of drought indicated by the U.S. Drought Monitor maps and the SMAP root-zone soil moisture deficit. Over the U.S. Southwest, monthly anomalies of soil moisture showed significant positive correlations with those of SMAP GPP (R^2 = 0.44, $p < 0.001$) and GOSIF ($R^2 = 0.76$, $p < 0.001$), demonstrating strong water availability constraints on plant productivity across dryland ecosystems. We further found that SMAP GPP and GOSIF captured the impact of drought on tower GPP and crop yield. Our results suggest that synergistic use of SMAP and OCO-2 data products can reveal the drought evolution and its impact on ecosystem productivity and carbon uptake at multiple spatial and temporal scales, and demonstrate the value of SMAP and OCO-2 for studying ecosystem function, carbon cycling, and climate change.

1. Introduction

Drought is a recurring natural phenomenon with widespread influence on both managed and natural ecosystems across the globe. Drought significantly affects terrestrial ecosystem productivity and carbon dynamics (Ciais et al., 2005; Xiao et al., 2009), and is found to be the major driver of declines in global net primary production (Chen et al., 2013; Zhao and Running, 2010). Exploring the responses of ecosystem productivity to drought can inform agricultural and forestry management and improve our understanding of the global carbon balance and carbon-climate feedbacks (Vicente-Serrano et al., 2013). In 2018, the U.S. Southwest experienced a severe and prolonged drought (Williams et al., 2020). This severe drought affected the vast majority of the region, including large parts of Colorado, New Mexico, Arizona, Utah, and Oregon, and smaller parts of northern North Dakota, West Texas, and southern California (NOAA National Centers for Environmental Information, 2018). The drought persistently impacted people, agriculture, and natural landscapes across the U.S. Southwest (Lindsey, 2019). For example, it intensified wildfires in Colorado and substantially reduced surface water supplies in New Mexico (NOAA

* Corresponding author.
E-mail address: j.xiao@unh.edu (J. Xiao).

https://doi.org/10.1016/j.rse.2020.112062
Received 9 March 2020; Received in revised form 25 August 2020; Accepted 30 August 2020
Available online 10 September 2020

National Centers for Environmental Information, 2018). However, it remains unclear how this drought affected ecosystem productivity and carbon uptake in the U.S. Southwest.

Optical-infrared remote sensing has traditionally been used to diagnose ecosystem responses to drought. For example, satellite-derived vegetation indices, including the normalized difference vegetation index (NDVI) (Rouse et al., 1974), enhanced vegetation index (EVI) (Huete et al., 2002), and normalized difference water index (NDWI) (Gao, 1996), are sensitive to water stress and have been commonly used for drought assessments (e.g., Gu et al., 2007; Ma et al., 2016; Samanta et al., 2010). These vegetation indices are used either as proxies for vegetation productivity or as key inputs to light use efficiency (LUE), data-driven, or diagnostic models (Xiao et al., 2019). The U.S. Southwest is water-limited (Biederman et al., 2017) and is dominated by dryland ecosystems (e.g., grassland, shrubland, and savanna), where traditional remote sensing techniques have been shown to have significant limitations for monitoring productivity (Smith et al., 2019). For example, the gross primary productivity (GPP) estimated from the Moderate Resolution Imaging Spectroradiometer (MODIS) only captured ~30% of the interannual variability of flux tower-based GPP across dryland sites across the region (Biederman et al., 2017). The relatively weak performance of proxies or primary production models based on remote sensing data in drylands could be attributed to weak signals due to sparse vegetation, effects of soil background, lack of sufficient data for model calibration, and inappropriate estimation of water stress effects (e.g., Smith et al., 2019). Fortunately, solar-induced chlorophyll fluorescence (SIF) measurements from new satellite platforms and operational soil moisture and productivity (GPP) records benefiting from low frequency (L-band) satellite microwave soil moisture retrievals have recently become available. These new satellite data streams can potentially provide new insights into vegetation physiological function and improve our understanding of drought-induced variations of productivity for a wide variety of ecosystem types including dryland ecosystems.

Satellite measurements of SIF have advanced the global monitoring of terrestrial photosynthesis in the past decade (Joiner et al., 2011; Frankenberg et al., 2011; Guanter et al., 2012; Joiner et al., 2013; Frankenberg et al., 2014; Köhler et al., 2018; Li and Xiao, 2019a; Mohammed et al., 2019; Ryu et al., 2019; Xiao et al., 2019). SIF is an optical signal emitted from excited chlorophyll molecules after light absorption (Baker, 2008). Diagnosing variations in SIF can reveal important information on plant biochemical and physiological status as well as availability of absorbed photosynthetically active radiation (APAR). Therefore, SIF has been found to be more sensitive to environment-induced photosynthetic variations compared to conventional vegetation indices that measure canopy greenness and chlorophyll abundance (Daumard et al., 2010; Li et al., 2018a; Yoshida et al., 2015).

SIF has been retrieved from several satellite instruments including the Greenhouse gases Observing SATellite (GOSAT) (Joiner et al., 2011; Frankenberg et al., 2011; Guanter et al., 2012), Global Ozone Monitoring Experiment-2 (GOME-2) (Joiner et al., 2013) and the SCanning Imaging Absorption spectroMeter for Atmospheric CHartographY (SCIAMACHY) (Joiner et al., 2016; Köhler et al., 2015). SIF from these satellite missions has been effective in estimating ecosystem productivity (Frankenberg et al., 2011; Guanter et al., 2012) and crop yield (Guan et al., 2016; Somkuti et al., 2020). SIF also showed strong potential for studying the effects of drought events (Li et al., 2018b; Parazoo et al., 2015; Sun et al., 2015; Yoshida et al., 2015) and heat waves (Song et al., 2018; Qiu et al., 2020) on ecosystems, although it was reported to have a weak performance in tracking GPP under short-term drought or heat waves when APAR showed little changes (Wohlfahrt et al., 2018; Wieneke et al., 2018). However, these gridded satellite SIF data have very coarse spatial resolutions (e.g., 0.5-2 degree), and they lack fine spatial details and are unsuitable for many applications (e.g., ecosystem-level studies). More recently, NASA launched the Orbiting Carbon Observatory-2 (OCO-2) on July 2, 2014, providing SIF retrievals with higher spatial resolution along orbits (1.3 × 2.25 km^2) and higher signal-to-noise ratio (Frankenberg et al., 2014) than previous satellite SIF data (e.g., GOME-2, SCIAMACHY, GOSAT). The footprint (i.e., size) of OCO-2 ground pixels is comparable to that of a typical eddy covariance (EC) flux tower, which allows for directly linking SIF with GPP from flux towers (henceforth "tower GPP") (Li et al., 2018a; Li et al., 2018c; Sun et al., 2017; Verma et al., 2017; Wood et al., 2017; Smith et al., 2018). However, due to the sparse sampling nature of OCO-2, regional to global scale studies rely on coarse spatial (e.g., 1–2 degree) and temporal (e.g., monthly) compositing of the fine-resolution OCO-2 soundings. To help resolve the limitations imposed from the coarse resolution SIF observations, global, fine-resolution and spatially continuous SIF datasets have been produced from OCO-2 SIF and other explanatory variables using machine learning methods (Zhang et al., 2018a; Yu et al., 2019; Li and Xiao, 2019a). These long-term, higher-resolution SIF datasets can support a broader range of applications (Li and Xiao, 2019b, 2020; Gang et al., 2020; Li et al., 2020) and therefore have greater potential in ecology, climate change, carbon cycle, remote sensing, and agriculture research.

Parallel to the advance of OCO-2 SIF, the SMAP mission launched in January 2015 by NASA provides global operational soil moisture retrievals with 1–3 day fidelity, moderate (9–36 km) spatial resolution and favorable accuracy (standard deviation of error less than 0.04 m^3/m^3) (Chan et al., 2018; Reichle et al., 2019). A key science goal of the SMAP mission is to improve capabilities for soil moisture and drought monitoring and for better understanding terrestrial water, energy, and carbon cycles. The SMAP L-band (1.41 GHz) microwave radiometer enhances sensitivity to surface soil moisture relative to higher frequency microwave sensors (Entekhabi et al., 2010). Recent findings found that soil moisture retrieved from L-band was more accurate than soil moisture retrievals from the Advanced Microwave Scanning Radiometer for the Earth Observing System (AMSR-E), the Advanced SCATterometer (ASCAT), and similar L-band soil moisture retrievals from the ESA Soil Moisture and Ocean Salinity (SMOS) mission (Chen et al., 2018; Kumar et al., 2018). Several studies also showed that the SMAP soil moisture was effective in monitoring meteorological and agricultural drought (Velpuri et al., 2016; Mishra et al., 2017; Mladenova et al., 2019) and improving global simulations of GPP (He et al., 2017) and evapotranspiration (Purdy et al., 2018). In addition to the microwave brightness temperature and surface soil moisture retrievals, the SMAP mission also provides model enhanced (Level 4) products including 3-hourly global estimates of root-zone (0–100 cm depth) soil moisture (L4SM) (Reichle et al., 2017) and daily Carbon (L4C) fluxes (GPP, ecosystem respiration, and net ecosystem exchange) (Jones et al., 2017).

Together, the SMAP and OCO-2 products can potentially provide new insight into ecosystem responses to drought through independent productivity assessments that account for the effects of available energy, canopy structure, atmospheric moisture deficit, and soil moisture related water supply controls on photosynthesis (Gonsamo et al., 2019). Previous studies have examined the impacts of drought on ecosystem productivity based on coarser-resolution satellite SIF (such as GOSAT and GOME-2) over U.S. central (Sun et al., 2015; Wang et al., 2016) and northern (He et al., 2019) Great Plains, Amazon (Li et al., 2018b; Zhang et al., 2018b), and Russia (Yoshida et al., 2015). However, studies using satellite SIF, especially those using finer-resolution SIF data, to examine the ecosystem productivity responses to drought in drylands are lacking (Qiu et al., 2020). In particular, it is unclear whether or to what extent OCO-2 SIF (or finer-resolution gridded SIF products based on OCO-2) and SMAP soil moisture and GPP products provide complementary information and are sensitive to drought in dryland ecosystems. Drought analysis usually requires simultaneous quantification of seasonal and interannual variations of vegetation and climate variables, and drought-related departures from climatological normals established from multi-year records. Heretofore, such applications have been constrained by the relatively short operational data records available from both SMAP and OCO-2. To date, SMAP and OCO-2 have acquired approximately five years of continuous overlapping global observations and finer-resolution SIF products based on OCO-2 data are also available recently, providing new opportunities to apply these observations to examine the impacts of drought on ecosystem productivity.

The objective of this study is to diagnose the responses of ecosystem productivity to the 2018 drought in the U.S using complementary satellite data from SMAP and OCO-2. We used the root-zone soil moisture from the SMAP L4SM product to characterize changes in plant-available soil moisture during the drought, and combined GPP from the SMAP L4C product (Jones et al., 2017) and the global, OCO-2 based SIF product (GOSIF) (Li and Xiao, 2019a) to evaluate regional productivity patterns and responses to drought and soil moisture variations. Synergistic use of these products in this study may provide enhanced ecological information and finer spatial and temporal fidelity than the previously used SMAP surface soil moisture observations and coarse-resolution OCO-2 SIF (Gonsamo et al., 2019), better elucidating how soil moisture and drought impact ecosystem productivity and carbon uptake. To our knowledge, our study is the first effort to diagnose how ecosystem productivity responded to the 2018 southwestern U.S. drought using SMAP and OCO-2 products, and to demonstrate the potential of these products for studies on ecosystem functioning, carbon cycling, and climate change.

2. Materials and methods

2.1. Data

We used maps from the U.S. Drought Monitor (USDM) to identify the intensity and spatial extent of the drought in 2018. The USDM drought index, produced weekly, is composited through expert synthesis of multiple existing drought metrics, including anomalies in rainfall, soil moisture, surface streamflow, crop conditions, and local impact reports from more than 450 observers across the country (Svoboda et al., 2002). The USDM aims to track the development and intensity of drought and to represent different types of drought impacts (e.g., meteorological, agricultural, socio-economic) across the U.S. The USDM maps have been widely used to benchmark various drought indices for evaluating their spatial and temporal patterns (Velpuri et al., 2016). The USDM has five categories of drought magnitude based on its historical percentile, including abnormally dry (D0, percentile $\leq$30%), moderate drought (D1, percentile $\leq$20%), severe drought (D2, percentile $\leq$10%), extreme drought (D3, percentile $\leq$5%), and exceptional drought (D4, percentile $\leq$2%). The 2% percentile of exceptional drought indicates that this type of drought is expected to occur only once or twice within 100 years. We used the shapefiles of the USDM drought intensity data (available at http://droughtmonitor.unl.edu) to characterize weekly drought conditions during the growing season in 2018. Drought mainly occurred in the U.S. Southwest, including Arizona, New Mexico, Colorado, Nevada, Utah, Oklahoma, and Texas (Fig. 1a-c), with the highest severity in the Four Corners region. We calculated the percentage of the areas affected by drought in these seven states (Fig. 1) and found that the 2018 drought began prior to April, peaked in summer (weeks 30–33), and was alleviated in late September and October (since week 38). For these states, more than 80% of the area (about 1,800,000 km^2) was affected by the drought (D0–D4) before the drought began to alleviate in late September (week 38), and more than 40% of the region (> 900,000 km^2) had at least severe drought (D2–D4) during weeks 13 to 36 (Fig. 1d).

We then used a variety of complementary observational datasets to examine how the drought affected regional ecosystem productivity. The datasets used included SMAP root-zone soil moisture, different satellite proxies of productivity (SMAP GPP, OCO-2 SIF, and GOSIF), along with vapor pressure deficit (VPD) and PAR from the Modern-Era Retrospective analysis for Research and Applications (MERRA-2), USDM maps, tower GPP from AmeriFlux Data, and county-level crop yield data from the National Agricultural Statistics Service (NASS). MODIS GPP (Zhao et al., 2005) and EVI (Huete et al., 2002) were also used as supplementary proxies of ecosystem productivity to understand the impact of the drought (See Methods in the Supplementary Material). Detailed information on SMAP and OCO-2 data including data period, spatial and temporal resolutions, and references is summarized in Table 1. Our analysis focused on the vegetation growing season from April to October over the period 2015–2018.

2.1.1. SMAP data

We used root-zone soil moisture from the SMAP L4SM product (Reichle et al., 2018) and GPP from the SMAP L4C product (Kimball et al., 2018) to examine drought-related impacts on ecosystem productivity. The L4SM product is generated from NASA GMAO GEOS-5 Catchment Land Surface Model predictions (Ducharne et al., 2000; Koster et al., 2000), adjusted using an ensemble Kalman filter assimilation of SMAP brightness temperatures. The L4SM framework benefits from spatial and temporal information in the SMAP observations and the meteorological forcing observations (e.g., precipitation), which constrains the land surface water and energy balance process descriptions encoded in the Catchment model (Reichle et al., 2019). The L4SM surface (0–5 cm) and root zone (0–100 cm) soil moisture estimates are produced globally, with 3-hourly and 9-km resolutions, and were validated against in situ measurements (Reichle et al., 2017; Reichle et al., 2019). We only used root-zone soil moisture in this study and hereinafter referred to the root-zone soil moisture simply as ‘soil moisture’.

The SMAP L4C product provides global daily operational estimates of GPP and other terrestrial carbon fluxes (NEE and ecosystem respiration) posted to the same 9-km global grid as the L4SM product. The L4C framework uses a satellite-based LUE model to compute GPP. The LUE term defines the daily rate of the conversion of APAR to vegetation biomass (Monteith and Moss, 1977); the LUE rate is reduced from a prescribed maximum under unfavorable environmental conditions including excessive atmospheric VPD, low root zone soil moisture levels, cold temperatures or frozen conditions (Kimball et al., 2008). The LUE response characteristics are uniquely calibrated for up to eight global Plant Functional Types (PFTs) using representative tower EC carbon flux measurements from global FLUXNET sites (Jones et al., 2017). Previous satellite-based ecosystem models characterize the moisture constraints on ecosystem productivity using VPD as a measure of atmospheric moisture deficit (Running et al., 2004) or precipitation as a soil moisture proxy (Potter et al., 1993). The L4C product determines GPP using L4SM root-zone soil moisture as an additional biophysical input, which along with VPD capture both atmospheric moisture demand and soil water supply constraints to productivity. Other L4C inputs include daily incoming solar radiation, humidity and temperature from the NASA GMAO GEOS-5 Forward Processing stream, MODIS land cover and 8-day *f*PAR operational (C6) time series. The L4C processing occurs at a 1-km resolution congruent with MODIS vegetation inputs, while subsampling from coarser ($\geq$9 km) daily soil moisture and meteorological inputs. The L4C outputs are then posted to a 9-km global grid, including GPP spatial means for each 9-km grid cell and up to eight PFT classes within each cell as derived from the 1-km processing. The nested grid format facilitates both landscape level and coarser global assessments. The SMAP L4C GPP record has favorable global accuracy and performance against an array of observational benchmarks, including independent tower carbon flux measurements and satellite SIF retrievals (Jones et al., 2017; Liu et al., 2019; Madani et al., 2017; Zhang et al., 2019).

2.1.2. OCO-2 data

OCO-2 SIF can depict vegetation photosynthetic activity, while spatially continuous, gridded OCO-2 SIF data can be directly generated from discrete SIF soundings based on coarse spatial and temporal resolutions only. Here, we mainly used the fine-resolution GOSIF product

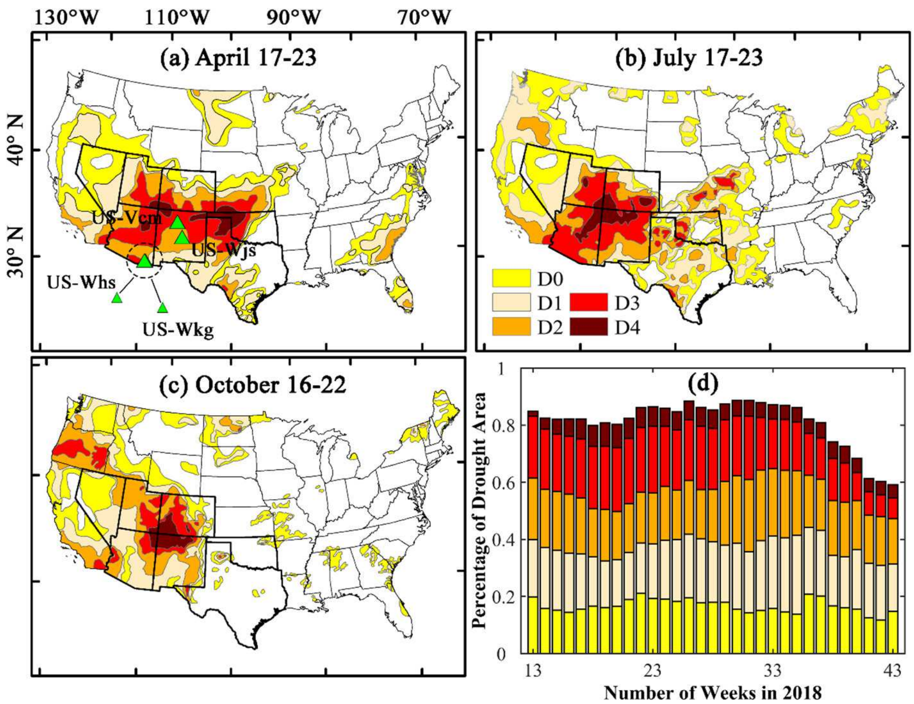

Fig. 1. Drought conditions over the Conterminous United States (CONUS) revealed by USDM. (a-c) Drought evolution in April, July, and October 2018; (d) The percentage of areas affected by drought (distinguished by different drought intensity) in seven states located in the U.S. Southwest, including Arizona, New Mexico, Colorado, Nevada, Utah, Oklahoma, and Texas, for each week from April to October during the growing season in 2018. Green triangles in (a) denote four eddy covariance (EC) flux tower sites used in this study. (For interpretation of the references to colour in this figure legend, the reader is referred to the web version of this article.)

Table 1
SMAP and OCO-2 data products used in this study.

Variables	Datasets	Data period	Spatial resolution	Temporal resolution	References
Root-zone soil moisture	SMAP L4SM	2015.4–2018	9 km	3-hourly	(Reichle et al., 2019)
GPP	SMAP L4C	2015.4–2018	9 km①	daily	(Jones et al., 2017)
SIF	OCO-2	2014.9–2018	1.3×2.25 km^2; ~1.5° ②	~Monthly③	(Frankenberg et al., 2014)
SIF④	GOSIF	2000–2018	0.05°	8-day	(Li and Xiao, 2019a)

① SMAP L4C outputs are gridded at 9-km resolution but retain sub-grid GPP means derived from finer (1-km) scale model operational processing for up to 8 plant functional type (PFT) classes within each grid cell . The 1-km processing is informed by MODIS *f*PAR and PFT inputs to the L4C model. This allows for more spatially matched and PFT consistent comparisons between L4C and tower GPP.
②,③ The ground-pixel size of OCO-2 SIF is 1.3×2.25 km^2. The coarse-resolution (such as 1.5° and monthly) OCO-2 SIF was directly aggregated from discrete OCO-2 SIF soundings, and the spatial and temporal resolutions depend on the tolerable spatial and temporal gaps and the number of soundings used.
④ The global, OCO-2 based SIF product (GOSIF) is a global, 0.05-degree SIF product derived from OCO-2 SIF soundings, MODIS EVI, and MERRA-2 reanalysis meteorological data using a data-driven (or machine learning) approach.

to examine variations in ecosystem productivity. The GOSIF record was produced from the original OCO-2 SIF retrievals using a data-driven (or machine-learning) based model that includes other finer-scale inputs as model predictors, including MODIS EVI and other environmental information that may regulate photosynthesis and fluorescence, including PAR, air temperature, and VPD from MERRA-2 (Li and Xiao, 2019a). The resulting GOSIF record has enhanced spatial and temporal resolution (0.05° and 8-day) and an extended length of record (2000-present) compared with coarse-resolution gridded SIF data directly aggregated from the original OCO-2 SIF retrievals (Li and Xiao, 2019a). The spatial patterns and seasonal cycles of GOSIF were consistent with those of coarse SIF data that were directly aggregated from OCO-2 SIF soundings, and were highly correlated with independent GPP data for 91 tower sites (Li and Xiao, 2019a). A detailed description of the GOSIF data (production, verification and application) can be found in Li and Xiao (2019a). The GOSIF data product is available at http://data.globalecology.unh.edu/.

2.1.3. Climate, flux tower, and crop yield data

We used monthly PAR and VPD obtained from the MERRA-2 (Gelaro et al., 2017), a NASA atmospheric reanalysis of the satellite era using the Goddard Earth Observing System Model, Version 5 (GEOS-5) with its Atmospheric Data Assimilation System (ADAS). Downwelling PAR was derived as the sum of the diffuse PAR and direct PAR. VPD was calculated from the surface temperature and specific humidity.

We explored whether SMAP GPP and GOSIF could capture drought-induced variations in productivity represented by EC flux tower GPP data and reported crop yield. We selected four flux sites (Fig. 1a) which all experienced the drought and had data available up to 2018, including Valles Caldera Mixed Conifer (US-Vcm, New Mexico) (Litvak, 2016a), Walnut Gulch Kendall Grasslands (US-Wkg, Arizona) (Scott et al., 2010; Scott, 2016a), Willard Juniper Savannah (US-Wjs, New Mexico) (Anderson-Teixeira et al., 2011; Litvak, 2016b) and Walnut Gulch Lucky Hills Shrub (US-Whs, Arizona) (Scott et al., 2006; Scott, 2016b). US-Vcm, a subalpine conifer site, experienced a very hot, stand-replacing burn in late May 2013, and is currently dominated by elderberry and aspen seedlings (1–2 m in height). The tower flux and meteorological data for these sites were obtained from the AmeriFlux tower network. The gap filling of EC data and partitioning of the NEE into GPP and ecosystem respiration were performed by the ReddyProc software (Wutzler et al., 2018).

We obtained county-level crop yield data for the seven southwestern U.S. states affected by the 2018 drought from the U.S. Department of Agriculture's (USDA) NASS. The reported end-of-season yields of the dominant crops (i.e., corn, soybean, winter wheat, sorghum and cotton) in each county from 2015 to 2018 were obtained from the NASS Quick

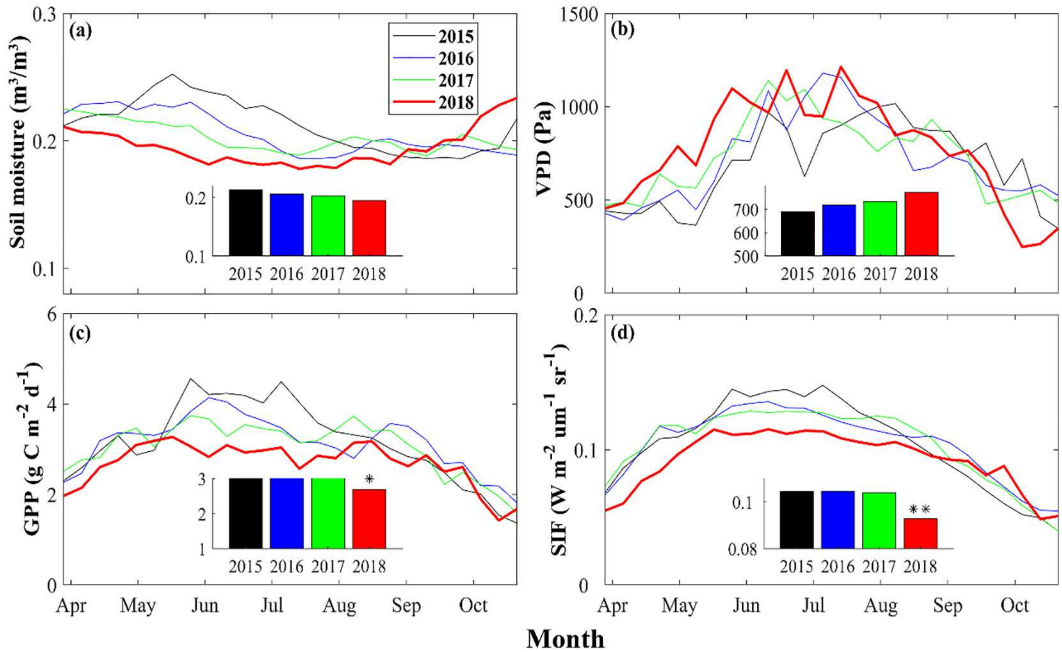

Fig. 2. Seasonal variations (8-day) of growing season (a) SMAP root-zone soil moisture, (b) VPD, (c) SMAP GPP, and (d) GOSIF from 2015 to 2018 for the seven states in the U.S. Southwest (including Arizona, New Mexico, Colorado, Nevada, Utah, Oklahoma, and Texas) affected by the 2018 drought. The red, heavy curve indicates the 2018 drought year. Bars in each sub-figure shows growing-season averaged soil moisture, VPD, GPP, and SIF. * in (c) indicates that GPP in 2018 was significantly lower than that in 2015–2017 ($p < 0.05$); while ** in (d) indicates that SIF in 2018 was significantly lower than that in 2015–2017 ($p < 0.01$). (For interpretation of the references to colour in this figure legend, the reader is referred to the web version of this article.)

Stats database (http://quickstats.nass.usda.gov). The NASS crop yield data provide a benchmark for evaluating the potential of SMAP GPP and GOSIF in monitoring the changes of crop production under water stress.

2.2. Analysis

We first compared seasonal (8-day) variations of MERRA-2 VPD, SMAP soil moisture, SMAP GPP, and GOSIF in the seven southwestern states severely affected by the 2018 drought (Fig. 1) over the growing season from 2015 to 2018. We also calculated the growing-season averages of these variables, and examined whether the ecosystem productivity in the 2018 drought significantly decreased using the one-way Analysis of Variance (ANOVA) method.

We then calculated the growing-season (April to October) averaged standardized anomalies of these variables during the 2018 drought year relative to their multiyear averages (2015–2018) to characterize the overall spatial effects of drought. For each variable, the standardized anomalies of each grid cell were calculated by subtracting the multiyear average from the value of the drought year, and then divided by the standard deviation of the variable over the four years. The anomalies based on this relatively short time period were consistent with those based on a longer time period from 2000 to 2018 (Figs. S1–2). Since SIF contains integrated information from vegetation structure (*f*PAR), radiation availability (PAR), and vegetation physiological states in response to altered environmental conditions (SIF_{yield}) (Sun et al., 2015), decomposing SIF into APAR and SIF_{yield} ($SIF = APAR \times SIF_{yield}$) can help clarify their individual contributions to the observed productivity anomalies during the drought. We also calculated growing-season averaged anomalies of APAR and SIF_{yield} to evaluate their relative contributions to the SIF anomalies. APAR was calculated by the product of *f*PAR (MCD15A2H) and PAR.

We also calculated the monthly standardized anomalies of SMAP GPP, OCO-2 SIF (i.e., the 1.5-degree and monthly SIF data), and GOSIF to examine whether these variables tracked the evolution of the soil moisture deficit in time and space. The USDM maps for May, July, and September 2018 were used as a reference for evaluating drought-related anomalies in the satellite metrics across the U.S. The USDM map for the middle week of each month (i.e., 15–21 May, 17–23 July, and 18–24 September) was used. The anomalies of APAR and SIF_{yield} were also calculated. To understand to what extent soil moisture controlled the variations of ecosystem productivity in the U.S. Southwest, we calculated the monthly anomalies of both pixel-level and regionally-averaged (i.e., seven drought-affected states defined in Fig. 1) SMAP soil moisture, SMAP GPP, GOSIF, SIF_{yield} and APAR during the growing season from 2015 to 2018. We then correlated the resulting soil moisture anomalies with those of SMAP GPP, GOSIF, SIF_{yield}, and APAR. Alternative ecosystem productivity metrics from the MODIS GPP and EVI were also used for comparison. To conduct the correlations on a per-pixel basis, all the variables were resampled to 9 km × 9 km.

We examined the 8-day variations of SMAP soil moisture, VPD, tower GPP, SMAP GPP, and GOSIF in the 2018 drought year relative to their multiyear averages, and assessed whether SMAP GPP and GOSIF could characterize the drought-induced reduction of tower GPP. For each of the three datasets (SMAP, GOSIF, and VPD), we extracted the time series for the grid cell in which each site was located. The L4C product includes both spatially-aggregated mean GPP for each 9-km grid cell and sub-grid GPP mean for each PFT within the cell. We extracted both L4C GPP estimates for each site, and only used the PFT-specific GPP matching the dominant vegetation type at each tower site for the drought analysis (Fig. S3).

Finally, we investigated whether the impact of the severe drought on the end-of-season crop yield across the southwestern states could also be captured by the SMAP GPP and GOSIF. We summed the total NASS reported crop yield of all dominant crops in each county, and normalized the yield into the standardized anomalies for each county for each year. The standardized anomalies of crop yield were then correlated with those of growing-season averages of SMAP GPP and GOSIF in each county. For SMAP GPP and GOSIF, only the cropland grid cells identified by the 0.05° MODIS land cover map - MCD12C1 were used to calculate the county-level averages. Any county with missing data for the dominant crops or with fewer than ten crop grid cells was excluded. A total of 57 counties mainly located in Texas, Oklahoma, and Colorado were used in this study. MODIS EVI was also included in the analyses for comparison purposes.

3. Results

3.1. Monitoring the impacts of the 2018 drought on ecosystem productivity with SMAP and OCO-2 data products

Over the seven drought-affected states in the U.S. Southwest (Fig. 1), soil moisture exhibited its lowest values and VPD had its highest values in 2018 (Fig. 2a, b). In response to this drought, ecosystem productivity significantly decreased over the U.S. Southwest. Specifically, SMAP GPP (ANOVA: $p < 0.05$) and GOSIF (ANOVA: $p < 0.01$) consistently showed their lowest values in 2018. From April to August, SMAP GPP and GOSIF tracked the soil moisture variations among years, while all of these variables showed decreasing trends from 2015 to 2018 (2015 > 2016 > 2017 > 2018). GOSIF had high consistency to other two productivity measures (Fig. S4) (GOSIF ~ SMAP GPP: $R^2 = 0.88$, $p < 0.001$; GOSIF ~ OCO-2 SIF: $R^2 = 0.90$, $p < 0.001$).

The 2018 growing season exhibited large anomalies in soil moisture, VPD, GPP, and GOSIF (Fig. 3). Large parts of the U.S. Southwest experienced severe drought (with 86.8% of the grid cells having negative anomalies in soil moisture and 87.9% of the grid cells having positive anomalies in VPD; Fig. 3a, b), resulting in suppressed ecosystem productivity (with 95.5% and 89% of the grid cells having negative anomalies in SMAP GPP and GOSIF, respectively; Fig. 3c, d). For this region dominated by arid and semi-arid ecosystems, the spatial patterns of productivity anomalies agreed well with anomalies in soil and atmospheric moisture conditions.

Widespread decreases across the U.S. Southwest were found for both APAR and SIF_{yield} (Fig. 4), suggesting that negative SIF anomalies were driven by simultaneous decreases in APAR and SIF_{yield}. Across the U.S., the SIF_{yield} anomalies were more consistent with the anomalous moisture conditions (Fig. 3a, b) than were the SIF or GPP anomalies in terms of spatial patterns (Fig. 3c, d).

The monthly anomalies of SMAP soil moisture, SMAP GPP, GOSIF, and corresponding USDM maps in May, July, and September 2018 are shown in Fig. 5. We found that SMAP soil moisture well captured the drought evolution and spatial spread as indicated by the USDM maps (first and second columns in Fig. 5). The drought had the most widespread impact in May, with negative soil moisture anomalies encompassing ~96.9% of the entire seven southwestern states. SMAP GPP and GOSIF showed large decreases in Arizona, New Mexico, and western Texas (Fig. 5). As the core drought area spread northwestward, negative anomalies of two productivity proxies were observed in Nevada, Utah, and Colorado in the following months, while the drought in Texas and New Mexico was alleviated by favorable moisture conditions (Fig. 5). GOSIF anomalies showed similar spatial and temporal patterns with the coarser-resolution OCO-2 SIF anomalies, but the latter was noisier (Fig. S5).

Over the U.S. Southwest, the monthly anomalies of GOSIF in large areas had strong correlations with those of soil moisture (Fig. 6a) during the growing season from 2015 to 2018. SMAP GPP showed weaker and slightly stronger sensitivity to soil moisture than did GOSIF and MODIS GPP, respectively (Fig. 6b, c). The high sensitivity of GOSIF to soil moisture variations was mainly contributed by SIF_{yield} and secondly by APAR (Figs. 6d, e and 7a, d, e). Like GOSIF, EVI was also strongly correlated with soil moisture (Fig. 6f). The correlations between regionally-averaged soil moisture and these six variables were generally consistent with those derived at the grid-cell scale (Fig. 7). GOSIF was more sensitive to the soil moisture variations than other five variables ($R^2 = 0.76$, $p < 0.001$), but its sensitivity was enhanced compared to that at the grid-cell scale. Similarly, MODIS GPP showed stronger response to the soil moisture variations than did SMAP GPP possibly because of the spatial integration.

3.2. SMAP and GOSIF captured the impacts of drought on flux tower GPP and crop yield

For all four tower sites (US-Vcm, US-Wkg, US-Whs, and US-Wjs), the 2018 drought started prior to the growing season with lower-than-normal soil moisture and higher VPD (Fig. 8), and the tower GPP

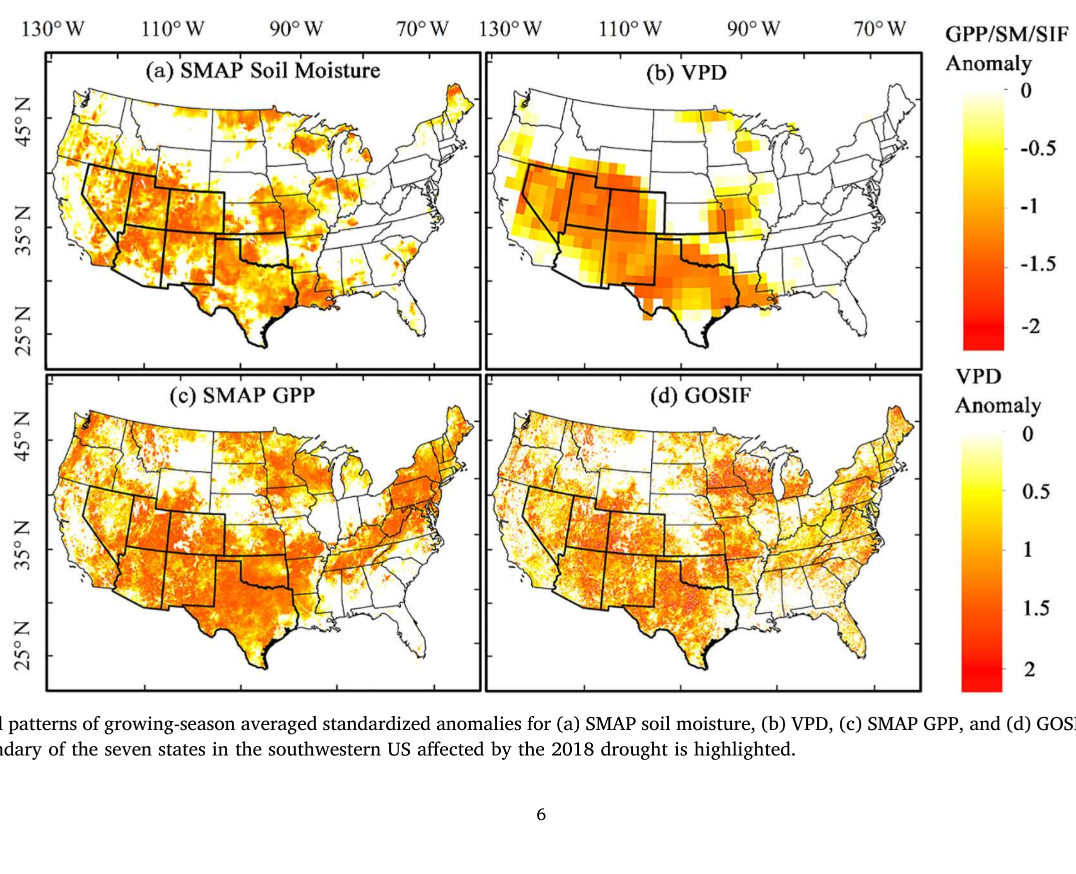

Fig. 3. The spatial patterns of growing-season averaged standardized anomalies for (a) SMAP soil moisture, (b) VPD, (c) SMAP GPP, and (d) GOSIF in 2018 over the CONUS. The boundary of the seven states in the southwestern US affected by the 2018 drought is highlighted.

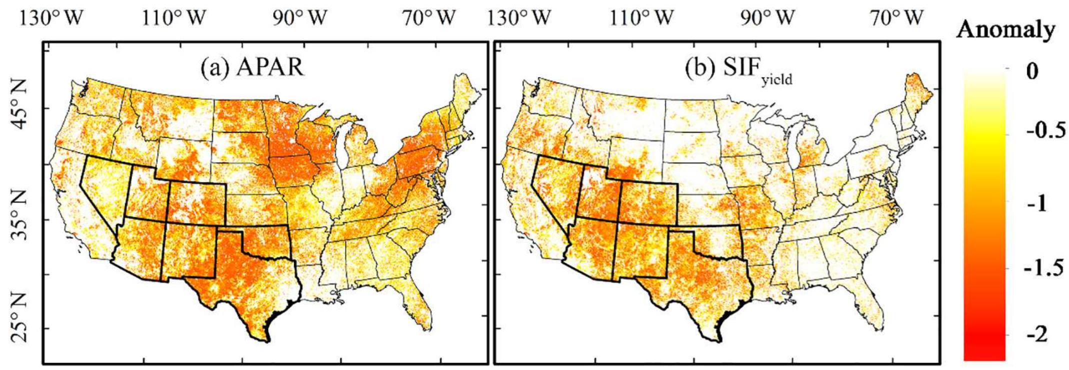

Fig. 4. The spatial patterns of the standardized anomalies for the growing-season averaged (a) APAR and (b) SIF$_{yield}$ in 2018 over the CONUS. The boundary of the seven states in the U.S. Southwest affected by the 2018 drought is highlighted.

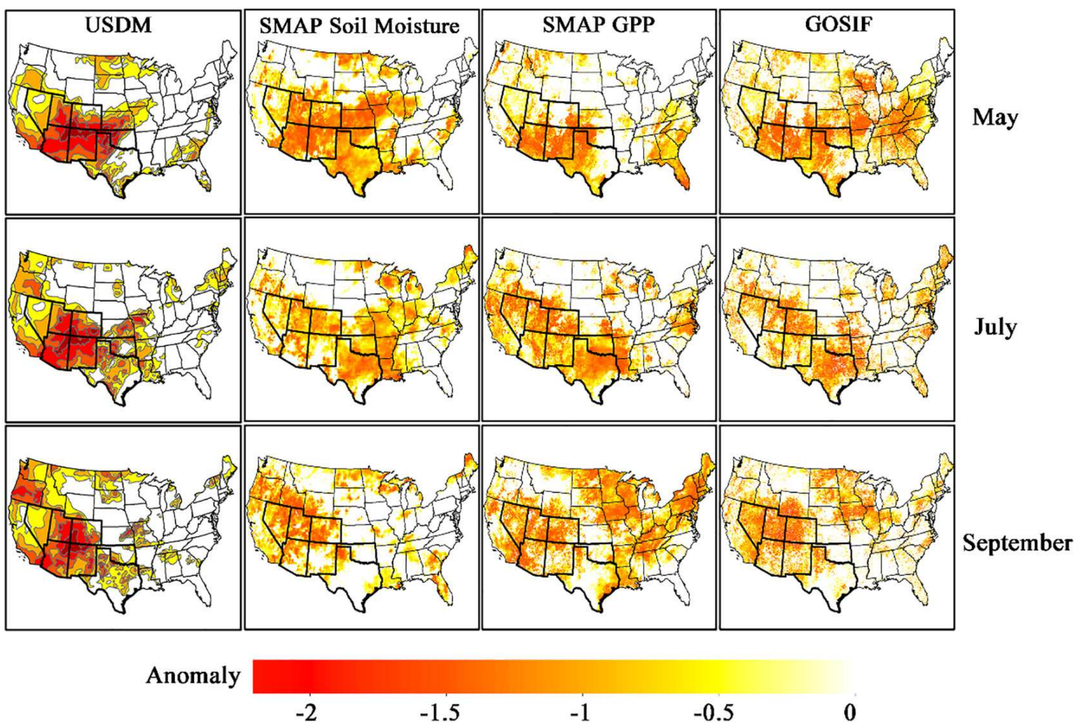

Fig. 5. The spatial patterns and temporal evolution of drought based on the USDM maps and monthly anomalies for SMAP soil moisture, SMAP GPP, and GOSIF in May, July, and September 2018 over the CONUS. The boundary of the seven states in the U.S. Southwest affected by the 2018 drought is highlighted.

generally decreased during the drought period. Tower GPP (and other proxies) returned to near-normal conditions around August for the US-Vcm and US-Wjs sites, and September for the US-Wkg and US-Whs sites, which corresponded to an increase in soil moisture. SMAP GPP and GOSIF generally captured the seasonal variability and drought-related impacts on tower GPP at the four sites. For US-Wjs, the recovery of tower GPP with drought relief was stronger than that was detected from SMAP GPP and GOSIF. Nevertheless, the magnitude of GPP decrease during the drought varied across sites and productivity proxies. For example, the US-Vcm experienced the largest decrease of soil moisture (~10.4%) among the four sites, leading to ~36% decrease of tower GPP compared to the average of 2015–2017, while the decrease of SMAP GPP and GOSIF was 2.1% and 9.6%, respectively. The decrease of productivity for other three sites was generally larger, with 18.5–24.4% decrease in tower GPP, 13.8–19.8% in SMAP GPP, and 21.0–34.2% in GOSIF, respectively.

Both GOSIF (R^2 = 0.46, p < 0.0001) and SMAP GPP (R^2 = 0.49, p < 0.0001) captured the impact of the 2018 drought on county-level crop yield (Fig. 9). The counties that were significantly affected by the drought (dark red circles on the lower left corner of Fig. 9a, b) had negative anomalies of crop yield and corresponding negative anomalies of GPP and SIF, while favorable soil moisture condition generally led to positive anomalies of yield and productivity. EVI also captured the variations of crop yield fairly well, and its performance was slightly lower than that of GOSIF and SMAP GPP (Fig. 9c).

4. Discussion

Our study showed that the soil moisture and GPP products derived from SMAP and the GOSIF product derived from OCO-2 could be effectively combined to monitor the 2018 southwestern U.S. drought and to assess its impacts on ecosystem productivity. We found that both SMAP GPP and GOSIF captured the changes in ecosystem productivity in response to the spatial spread and temporal evolution of the negative anomalies in soil moisture to a large extent. The consistency between these products has important implications. First, SIF and photosynthesis are mechanistically linked (Baker, 2008), whereby SIF contains additional environmental information that extends beyond conventional

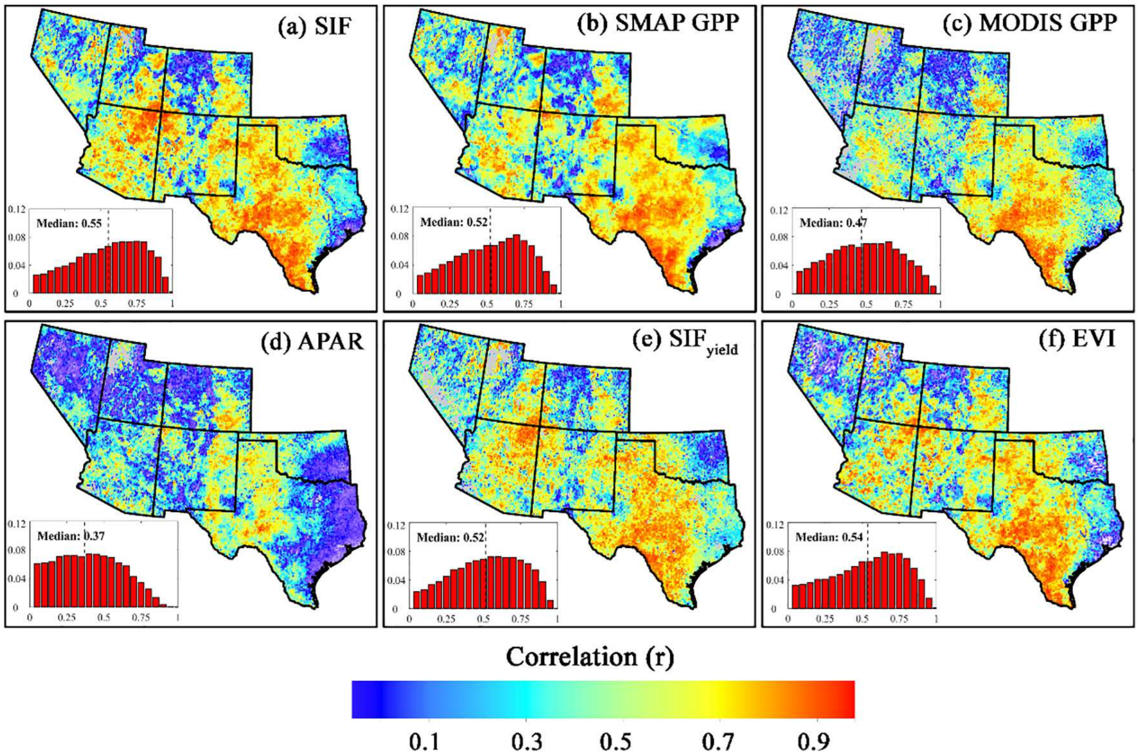

Fig. 6. Correlation coefficients (r) between monthly anomalies of SMAP soil moisture and anomalies of (a) GOSIF, (b) SMAP GPP, (c) MODIS GPP, (d) APAR, (e) SIF_{yield} (e), and (f) EVI for the seven drought-affected states from April to October over the period 2015–2018. The bars in each inset show the probability density of r, and the vertical lines indicate the median r.

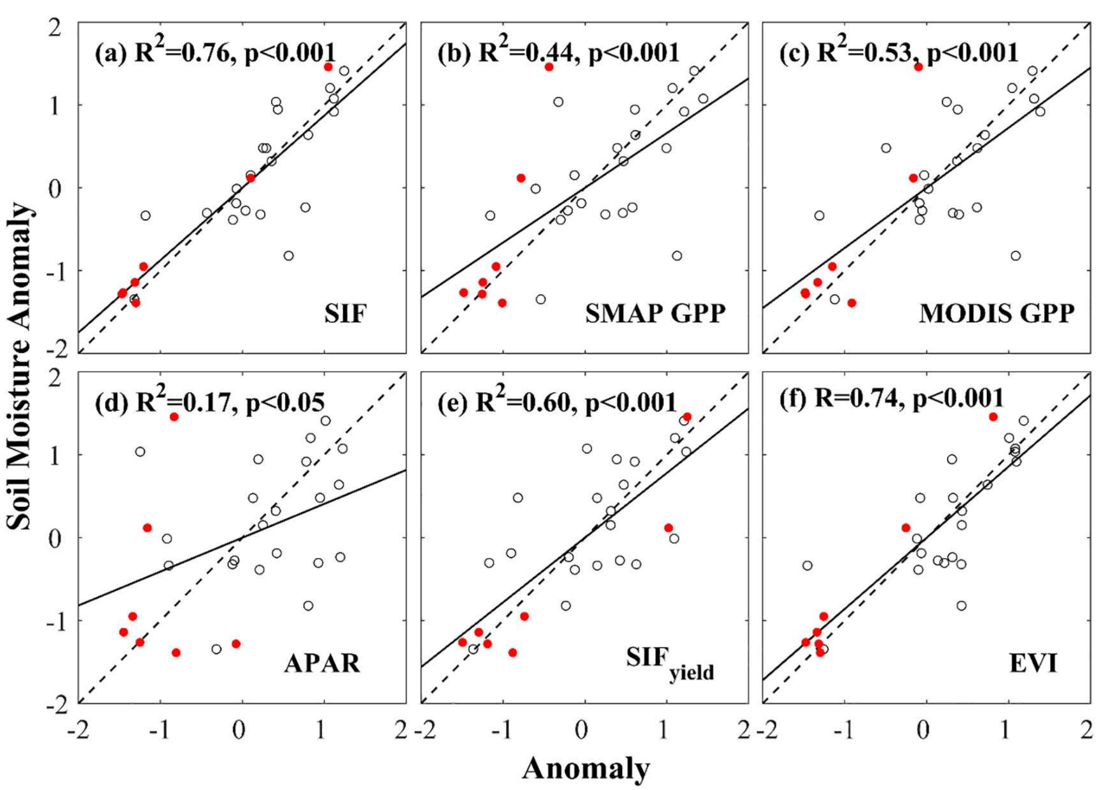

Fig. 7. Relationships between monthly anomalies of SMAP soil moisture and anomalies of (a) GOSIF, (b) SMAP GPP, (c) MODIS GPP, (d) APAR, (e) SIF_{yield}, and (f) EVI. Each circle represents the anomaly of the regional average of variables within the seven drought-affected states from April to October over 2015–2018 with filled red circles denoting the 2018 drought year. Solid and dashed lines denote the regression and 1:1 lines, respectively. (For interpretation of the references to colour in this figure legend, the reader is referred to the web version of this article.)

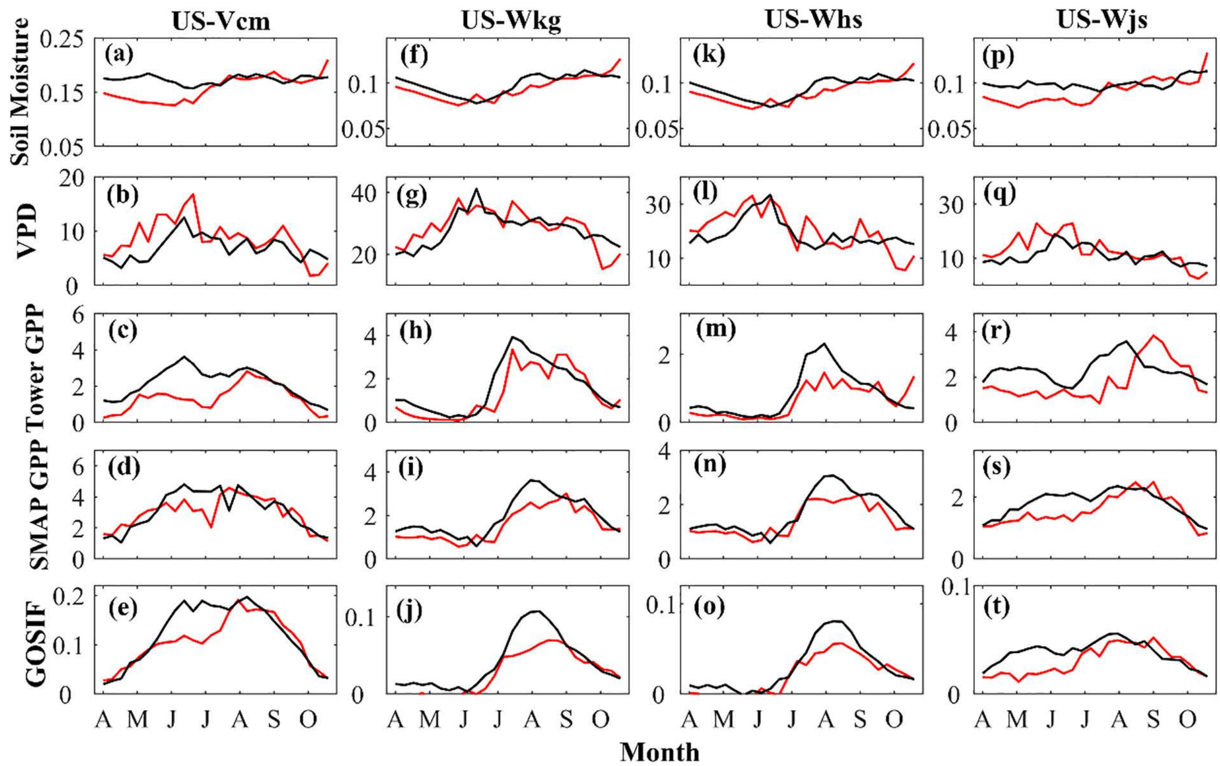

Fig. 8. The seasonal cycles of SMAP soil moisture (m^3/m^3), VPD (hPa), tower GPP (g C m^{-2} d^{-1}), SMAP GPP (g C m^{-2} d^{-1}) and GOSIF (W m^{-2} μm^{-1} sr^{-1}) at four EC flux sites. The red lines stand for the 8-day variations in the growing season during the 2018 drought year, while the black lines denote the averages of the normal years. (For interpretation of the references to colour in this figure legend, the reader is referred to the web version of this article.)

vegetation indices (Li et al., 2018a; Li et al., 2018c). Previous studies have reported that SIF had a stronger relationship with GPP compared with vegetation indices including NDVI, EVI, and NIR_v (Li et al., 2018c; Smith et al., 2018; Yang et al., 2015). Other studies also reported an enhanced ability of SIF in monitoring the responses of ecosystem productivity to drought and heat waves (Yoshida et al., 2015; Wang et al., 2016; Song et al., 2018; Qiu et al., 2020). We found that GOSIF and OCO-2 SIF were able to track the spatio-temporal variations of SMAP GPP, again confirming the strong relationship between SIF and photosynthesis. SMAP data alone can be applied to diagnose the drought impact on ecosystem productivity with soil moisture characterizing drought and GPP measuring productivity variations. However, these two products are not independent since the L4C GPP is derived using SMAP root zone soil moisture as a model input. Therefore, combining GOSIF (or OCO-2 SIF) and SMAP GPP as independent measures of productivity can provide more robust insight into the impact of drought on ecosystem productivity. Second, GOSIF showed similar spatio-temporal variations with the coarse-resolution SIF directly aggregated from OCO-2 soundings during the drought. The GOSIF record has much finer spatial and temporal resolutions than the coarse-resolution gridded SIF that were directly aggregated from OCO-2 SIF soundings. The higher temporal resolution (e.g., 8-day) observations provided by the SMAP and GOSIF data also enabled more consistent comparisons with the USDM maps, which can better depict the drought evolution and associated ecosystem impacts for more timely drought risk and mitigation assessments.

We found that GOSIF was more sensitive to soil moisture variations compared to SMAP GPP and MODIS GPP (Figs. 6-7). This higher

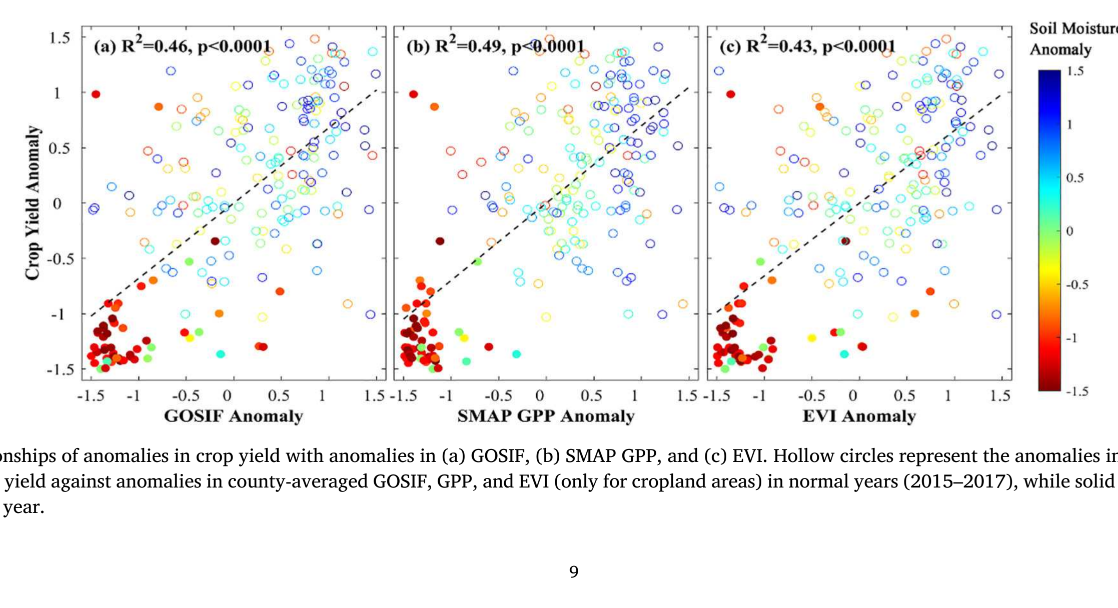

Fig. 9. Relationships of anomalies in crop yield with anomalies in (a) GOSIF, (b) SMAP GPP, and (c) EVI. Hollow circles represent the anomalies in county-level end of season crop yield against anomalies in county-averaged GOSIF, GPP, and EVI (only for cropland areas) in normal years (2015–2017), while solid circles denote the 2018 drought year.

sensitivity was mainly contributed by the $SIF_{yield,}$ which was effective in capturing the drought conditions. Our results are consistent with the findings of several previous studies (Yoshida et al., 2015; Sun et al., 2015; Li et al., 2018b). For example, Li et al., 2018b found that SIF_{yield} largely responded to precipitation and VPD anomalies, and the correlation decreased as the region became wetter. Wang et al. (2020) showed that the spatial pattern of SIF_{yield} during the growing season could be largely explained by the spatial variability of precipitation. The U.S. Southwest is dominated by arid and semi-arid ecosystems, and therefore the SIF_{yield} was expected to be largely affected by the lower soil moisture. SIF_{yield} was jointly determined by fluorescence yield (Φ_F) and escape ratio (f_{esc}, the fraction of SIF photons escaping from canopy) (Zeng et al., 2019). More recent studies further found that the f_{esc} was strongly correlated with LUE (Dechant et al., 2020) and may be the major driver of the observed variability in SIF_{yield} (Wang et al., 2020). Compared to SIF_{yield}, APAR had lower sensitivity to the soil moisture variations in this region.

The site-level analyses further confirmed the stronger relationships between GOSIF (SIF_{yield}) and tower GPP. APAR overall showed slightly lower correlation with tower GPP than EVI alone (Table S1), indicating that PAR was not the dominant driver in controlling the productivity for these dryland ecosystems (Nemani et al., 2003). For the US-Whs and US-Wjs sites, in particular, the weaker relationship found between the SMAP/MODIS GPP and tower GPP was generally accompanied by a weaker relationship between APAR and tower GPP (Table S1). Although GOSIF (or SIF in general) shared the same APAR term as SMAP/MODIS GPP, SIF_{yield} had stronger relationship with tower GPP (or tower LUE) compared to SMAP/MODIS LUE, and thereby GOSIF had better agreement with tower GPP than did SMAP/MODIS GPP (Table S1). This indicates that the representation of the LUE term for both GPP products can be further improved for dryland ecosystems.

Our study provides insight into the relative regulation of APAR and SIF_{yield} on the variations of ecosystem productivity during drought. Several studies found a strong relationship between APAR and SIF (or GPP) (Sun et al., 2015; Li et al., 2018b; Yang et al., 2018). Over the U.S. Southwest dominated by dryland ecosystems, the decrease of SIF during the 2018 drought was mainly driven by SIF_{yield} and secondly by APAR. For some other regions such as the Corn Belts and Northeast U.S., soil moisture was higher in 2018 while SMAP GPP and GOSIF decreased (Fig. 3). This inconsistency was mainly driven by lower APAR (Fig. 4a). APAR instead of soil moisture conditions or SIF_{yield} dominated the variations of ecosystem productivity in parts of the Corn Belt (e.g., Iowa, Minnesota, Wisconsin) and the Appalachian Mountains. We found that these regions experienced widespread decrease of APAR in 2018, resulting from much reduced PAR. Solar radiation is a primary climate driver controlling plant growth (Nemani et al., 2003), and therefore the APAR decrease resulted in lower productivity in these regions. This was consistent with previous findings that highlighted the effects of solar radiation on plant photosynthesis (Myneni et al., 2007; Nemani et al., 2003). SMAP GPP showed more substantial reduction than GOSIF in these regions, coinciding with the observed negative APAR anomalies; while GOSIF neutralized these negative anomalies by including information from SIF_{yield}. Previous studies reported either stronger GPP-SIF relationships over GPP-APAR (or SIF-APAR) relationships (Zhang et al., 2016; Li et al., 2018a) or stronger SIF-APAR relationships over SIF-GPP (or APAR-GPP) relationships (Yang et al., 2018), which depended on the relationship between LUE and SIF_{yield} (strong or weak). The stronger spatial consistency between SMAP GPP and APAR than that between GOSIF and APAR was also found at the monthly scale (Fig. S5), indicating that LUE from SMAP provided less information on the drought-induced variations of productivity than the SIF_{yield}. This difference may be closely related to the different methods for SMAP GPP (a LUE model) and GOSIF (a data-driven approach), and the potential uncertainty associated with input data or modeling/data-driven approach (Jones et al., 2017; Li and Xiao, 2019a).

Several studies have indicated that the satellite-derived SIF based on GOSAT, GOME-2 (Guanter et al., 2014; Guan et al., 2016; Zhang et al., 2018; Somkuti et al., 2020) or more recently the TROPOspheric Monitoring Instrument (TROPOMI) (He et al., 2020) had potential to diagnose drought impacts on crop yield or improve the estimation of crop yield. In our study, SMAP GPP and GOSIF were able to characterize variations in county-level crop yield for the southwestern U.S., and had potential to capture drought-induced crop yield loss. Nevertheless, they still poorly captured the reported year-to-year variations of crop yield in a few counties, which may be due to one or more factors, including the short period of data used, the limitation in current spatial resolution of the data, uncertainty from estimated SIF or GPP, and biases of the county-level crop yield (Sadras et al., 2014). It should be noted that our analysis only covered four years, thus limiting the sampling of interannual variability in the present study. Inclusion of more data (longer records or additional regions) that encompass a greater variety of anomalously dry and wet conditions would likely improve the relationships. In addition, for three counties, we found that both crop yield and SMAP GPP declined in the 2018 drought, while GOSIF slightly increased (Fig. 9). The negative anomalies of SMAP GPP were mainly contributed by largely reduced soil moisture, while SIF_{yield} did not well capture the drought condition. This suggested that although SIF_{yield} showed an overall strong response to the soil moisture condition, integrating SMAP soil moisture into the prediction of GOSIF in the near future may further improve the ability of GOSIF for monitoring drought.

We also found that the variations of yield for irrigated crops were weakly related to SMAP GPP and GOSIF, while the yield of rainfed crops had much higher sensitivity to the variations of soil moisture, and thus strongly correlated with SMAP GPP and GOSIF (Fig. S10). This confirmed the findings of previous studies that rainfed crops are more vulnerable to climate change or drought than irrigated crops (Li et al., 2015; Ozelkan et al., 2016). Although GOSIF (or SMAP GPP) has finer spatial resolution than previous coarse-resolution SIF records, it is still inadequate for delineating finer field scale crop types and management practices (e.g., irrigation), considering that the U.S. Southwest has more mixed and smaller crop patches compared with the Corn Belt in Midwestern U.S. Higher resolution SIF available in the near future, such as the FLuorescence EXplorer (FLEX, 300 m) (Drusch et al., 2016), will likely help eliminate this gap. Future work may also examine how SMAP GPP (associated with soil moisture scalar) and GOSIF (associated with uncertainty in three climatic variables) over- or under-estimate the impact of drought on crop yield for a variety of crop types over different agricultural regions.

Our results not only highlight the consistency between SMAP GPP and GOSIF (or OCO-2 SIF) in monitoring the responses of ecosystem productivity to drought but also clearly reveal their individual advantages and disadvantages among the three products or beyond (such as MODIS EVI or GPP). Among these products, GOSIF performed the best in capturing the changes in ecosystem productivity in response to the variations of soil moisture during the drought. The finer-resolution (0.05°) GOSIF (Li and Xiao, 2019a) derived from discrete OCO-2 SIF soundings enables enhanced delineation of drought or heat waves related impacts on regional ecosystems more commensurate with the scale of in situ tower EC observations compared with coarse-resolution GOSAT and GOME-2 SIF (Yoshida et al., 2015; Sun et al., 2015; Li et al., 2018b; Qiu et al., 2020). The additional environmental information such as VPD, air temperature (or land surface temperature), and PAR included in producing GOSIF may help improve the sensitivity of SIF to GPP. The uncertainty associated with these input data, however, can also lead to biases in the resulting gridded SIF products. For dryland ecosystems, previous studies reported a much stronger ability of SIF in capturing the interannual variation of tower GPP (Smith et al., 2018; Zuromski et al., 2018) or water and heat stresses (Qiu et al., 2020) over EVI. Our findings showed that the EVI was also able to capture the drought condition and its impact on tower GPP and crop yield (Table S1 and Fig. 9 and Fig. S6), although with slightly lower performance than

GOSIF. The highest temporal resolution of SMAP data (up to 3-hourly for soil moisture and daily for GPP and NEE) among all other data examined, enables sub-daily or daily analysis, which can better detect dynamic weather impacts to ecosystems including transient wetting and drying events represented in the tower EC record. Compared with MODIS GPP, SMAP GPP may have improved the GPP estimation to a certain extent by including soil moisture information to the LUE model (Table S1). Incorporating SIF (SIF_{yield}) as a novel proxy of LUE may further improve SMAP or other satellite GPP products.

5. Conclusions

This study explored the potential of SMAP and OCO-2 based data in monitoring the responses of ecosystem productivity to the 2018 drought in the U.S. Southwest. We assessed the consistency of the spatial extent and temporal evolution between SMAP root-zone soil moisture estimates and two ecosystem productivity proxies, SMAP GPP and OCO-2 based finer-resolution SIF (GOSIF), and also examined whether SMAP GPP and GOSIF could capture the impact of drought on flux tower GPP and NASS reported crop yield. Our results showed that over the drought-affected states in the U.S. Southwest, SMAP GPP and GOSIF responded strongly to anomalies in VPD and soil moisture. These proxies also well captured the drought dynamics indicated by the USDM drought maps. The drought-related decrease in SIF resulted from decreases in both APAR and SIF_{yield}. The regionally-averaged soil moisture showed significant positive correlations with SMAP GPP ($R^2 = 0.44$, $p < 0.001$) and GOSIF ($R^2 = 0.76$, $p < 0.001$), demonstrating that soil water availability had a strong control on ecosystem productivity in dryland ecosystems. We also found that SMAP GPP and GOSIF were able to characterize the variations of flux tower GPP for different ecosystems, and largely captured the anomalous crop yield reductions during the drought. The synergistic use of these data revealed the responses of ecosystem productivity to the changes in APAR and soil moisture during the 2018 drought across the U.S., and also provided better clarification of drought impacts on ecosystems at various spatial and temporal resolutions than the use of any single data source. Our study provides a regional application demonstration of these newer satellite data for assessing the impacts of drought on ecosystem productivity and carbon uptake, while the widespread application and validation of these data in other parts of the world for diagnosing other drought events require further exploration. Finer-resolution SIF observations from next generation satellite sensors are expected to offer enhanced capabilities for more accurately monitoring ecosystem productivity and drought impacts, particularly in heterogeneous regions.

Author contributions

X. Li and J. Xiao designed the research, conducted the analysis, and wrote the manuscript. J.S. Kimball, R.H. Reichle, R.L. Scott, M.E. Litvak, G. Bohrer, and C. Frankenberg contributed data and to the writing of the manuscript.

Declaration of Competing Interest

None.

Acknowledgements

This study was supported by the National Aeronautics and Space Administration (NASA) (PI Jingfeng Xiao: Climate Indicators and Data Products for Future National Climate Assessments - Grant No. NNX16AG61G and Carbon Cycle Science Program - Grant No. NNX14AJ18G) and National Science Foundation (NSF) (PI Jingfeng Xiao: Macrosystem Biology & NEON-Enabled Science program - Grant No. DEB-2017870). The contribution of J.S.K. was supported by NASA Grant No. NNH15ZDA001N and NNX15AT74A. R.R. was supported by the SMAP project. We thank the OCO-2 and SMAP science teams for making OCO-2 SIF and SMAP root-zone soil moisture and GPP data available and USDA-NASS for providing crop yield data. We also thank the principal investigators and other research personnel of the four AmeriFlux sites for making the flux data available. Funding for AmeriFlux data resources was provided by the U.S. Department of Energy's Office of Science. We thank the five anonymous reviewers for their two rounds of insightful and constructive comments on our manuscript.

Appendix A. Supplementary data

Supplementary material to this article can be found online at https://doi.org/10.1016/j.rse.2020.112062.

References

Anderson-Teixeira, K.J., Delong, J.P., Fox, A.M., Brese, D.A., Litvak, M.E., 2011. Differential responses of production and respiration to temperature and moisture drive the carbon balance across a climatic gradient in New Mexico. Glob. Chang. Biol. 17, 410–424.

Baker, N.R., 2008. Chlorophyll fluorescence: a probe of photosynthesis in vivo. Annu. Rev. Plant Biol. 59, 89–113.

Biederman, J.A., Scott, R.L., Bell, T.W., Bowling, D.R., Dore, S., Garatuza-Payan, J., Kolb, T.E., Krishnan, P., Krofcheck, D.J., Litvak, M.E., 2017. CO 2 exchange and evapotranspiration across dryland ecosystems of southwestern North America. Glob. Chang. Biol. 23, 4204–4221.

Chan, S., Bindlish, R., O'Neill, P., Jackson, T., Njoku, E., Dunbar, S., Chaubell, J., Piepmeier, J., Yueh, S., Entekhabi, D., 2018. Development and assessment of the SMAP enhanced passive soil moisture product. Remote Sens. Environ. 204, 931–941.

Chen, T., Werf, G., Jeu, R., Wang, G., Dolman, A., 2013. A global analysis of the impact of drought on net primary productivity. Hydrol. Earth Syst. Sci. 17, 3885–3894.

Chen, F., Crow, W.T., Bindlish, R., Colliander, A., Burgin, M.S., Asanuma, J., Aida, K., 2018. Global-scale evaluation of SMAP, SMOS and ASCAT soil moisture products using triple collocation. Remote Sens. Environ. 214, 1–13.

Ciais, P., Reichstein, M., Viovy, N., Granier, A., Ogée, J., Allard, V., Aubinet, M., Buchmann, N., Bernhofer, C., Carrara, A., 2005. Europe-wide reduction in primary productivity caused by the heat and drought in 2003. Nature 437, 529–533.

Daumard, F., Champagne, S., Fournier, A., Goulas, Y., Ounis, A., Hanocq, J.-F., Moya, I., 2010. A field platform for continuous measurement of canopy fluorescence. IEEE Trans. Geosci. Remote Sens. 48, 3358–3368.

Dechant, B., Ryu, Y., Badgley, G., Zeng, Y., Berry, J.A., Zhang, Y., Goulas, Y., Li, Z., Zhang, Q., Kang, M., 2020. Canopy structure explains the relationship between photosynthesis and sun-induced chlorophyll fluorescence in crops. Remote Sens. Environ. 241, 111733.

Drusch, M., Moreno, J., Del Bello, U., Franco, R., Goulas, Y., Huth, A., Kraft, S., Middleton, E.M., Miglietta, F., Mohammed, G., 2016. The fluorescence explorer mission concept—ESA's earth explorer 8. IEEE Trans. Geosci. Remote Sens. 55, 1273–1284.

Ducharne, A., Koster, R.D., Suarez, M.J., Stieglitz, M., Kumar, P., 2000. A catchment-based approach to modeling land surface processes in a general circulation model: 2. Parameter estimation and model demonstration. J. Geophys. Res.-Atmos. 105, 24823–24838.

Entekhabi, D., Njoku, E.G., O'Neill, P.E., Kellogg, K.H., Crow, W.T., Edelstein, W.N., Entin, J.K., Goodman, S.D., Jackson, T.J., Johnson, J., 2010. The soil moisture active passive (SMAP) mission. Proc. IEEE 98, 704–716.

Frankenberg, C., Fisher, J.B., Worden, J., Badgley, G., Saatchi, S.S., Lee, J.E., Toon, G.C., Butz, A., Jung, M., Kuze, A., 2011. New global observations of the terrestrial carbon cycle from GOSAT: patterns of plant fluorescence with gross primary productivity. Geophys. Res. Lett. 38.

Frankenberg, C., O'Dell, C., Berry, J., Guanter, L., Joiner, J., Köhler, P., Pollock, R., Taylor, T.E., 2014. Prospects for chlorophyll fluorescence remote sensing from the orbiting carbon Observatory-2. Remote Sens. Environ. 147, 1–12.

Gang, C., Pan, S., Tian, H., Wang, Z., Xu, R., Bian, Z., Pan, N., Yao, Y., Shi, H., 2020. Satellite observations of forest resilience to hurricanes along the northern Gulf of Mexico. For. Ecol. Manag. 472, 118243.

Gao, B.-C., 1996. NDWI—A normalized difference water index for remote sensing of vegetation liquid water from space. Remote Sens. Environ. 58, 257–266.

Gelaro, R., McCarty, W., Suárez, M.J., Todling, R., Molod, A., Takacs, L., Randles, C.A., Darmenov, A., Bosilovich, M.G., Reichle, R., 2017. The modern-era retrospective analysis for research and applications, version 2 (MERRA-2). J. Clim. 30, 5419–5454.

Gonsamo, A., Chen, J.M., He, L., Sun, Y., Rogers, C., Liu, J., 2019. Exploring SMAP and OCO-2 observations to monitor soil moisture control on photosynthetic activity of global drylands and croplands. Remote Sens. Environ. 232, 111314.

Gu, Y., Brown, J.F., Verdin, J.P., Wardlow, B., 2007. A five-year analysis of MODIS NDVI and NDWI for grassland drought assessment over the central Great Plains of the United States. Geophys. Res. Lett. 34.

Guan, K., Berry, J.A., Zhang, Y., Joiner, J., Guanter, L., Badgley, G., Lobell, D.B., 2016.

Improving the monitoring of crop productivity using spaceborne solar-induced fluorescence. Glob. Chang. Biol. 22, 716–726.
Guanter, L., Frankenberg, C., Dudhia, A., Lewis, P.E., Gómez-Dans, J., Kuze, A., Suto, H., Grainger, R.G., 2012. Retrieval and global assessment of terrestrial chlorophyll fluorescence from GOSAT space measurements. Remote Sens. Environ. 121, 236–251.
Guanter, L., Zhang, Y., Jung, M., Joiner, J., Voigt, M., Berry, J.A., Frankenberg, C., Huete, A.R., Zarco-Tejada, P., Lee, J.-E., 2014. Global and time-resolved monitoring of crop photosynthesis with chlorophyll fluorescence. Proc. Natl. Acad. Sci. 111, E1327–E1333.
He, L., Chen, J.M., Liu, J., Bélair, S., Luo, X., 2017. Assessment of SMAP soil moisture for global simulation of gross primary production. J. Geophys. Res. Biogeosci. 122, 1549–1563.
He, M., Kimball, J.S., Yi, Y., Running, S., Guan, K., Jensco, K., Maxwell, B., Maneta, M., 2019. Impacts of the 2017 flash drought in the US northern plains informed by satellite-based evapotranspiration and solar-induced fluorescence. Environ. Res. Lett. 14, 074019.
He, L., Magney, T., Dutta, D., Yin, Y., Köhler, P., Grossmann, K., Stutz, J., Dold, C., Hatfield, J., Guan, K., 2020. From the ground to space: using solar-induced chlorophyll fluorescence to estimate crop productivity. Geophys. Res. Lett. 47 (e2020GL087474).
Huete, A., Didan, K., Miura, T., Rodriguez, E.P., Gao, X., Ferreira, L.G., 2002. Overview of the radiometric and biophysical performance of the MODIS vegetation indices. Remote Sens. Environ. 83, 195–213.
Joiner, J., Yoshida, Y., Vasilkov, A., Middleton, E., 2011. First observations of global and seasonal terrestrial chlorophyll fluorescence from space. Biogeosciences 8, 637–651.
Joiner, J., Guanter, L., Lindstrot, R., Voigt, M., Vasilkov, A., Middleton, E., Huemmrich, K., Yoshida, Y., Frankenberg, C., 2013. Global monitoring of terrestrial chlorophyll fluorescence from moderate spectral resolution near-infrared satellite measurements: methodology, simulations, and application to GOME-2. Atmos. Measur. Techniq. 6, 2803–2823.
Joiner, J., Yoshida, Y., Guanter, L., Middleton, E.M., 2016. New methods for the retrieval of chlorophyll red fluorescence from hyperspectral satellite instruments: simulations and application to GOME-2 and SCIAMACHY. Atmos. Measur. Techniq. 9.
Jones, L.A., Kimball, J.S., Reichle, R.H., Madani, N., Glassy, J., Ardizzone, J.V., Colliander, A., Cleverly, J., Desai, A.R., Eamus, D., 2017. The SMAP level 4 carbon product for monitoring ecosystem land–atmosphere CO 2 exchange. IEEE Trans. Geosci. Remote Sens. 55, 6517–6532.
Kimball, J.S., Jones, L.A., Zhang, K., Heinsch, F.A., McDonald, K.C., Oechel, W.C., 2008. A satellite approach to estimate land–atmosphere CO2 exchange for boreal and Arctic biomes using MODIS and AMSR-E. IEEE Trans. Geosci. Remote Sens. 47, 569–587.
Kimball, J.S., Jones, L.A., Kundig, T., Reichle, R., 2018. *SMAP L4 Global Daily 9 km EASE-Grid Carbon Net Ecosystem Exchange, Version 4*. Boulder, Colorado USA. NASA National Snow and Ice Data Center Distributed Active Archive Center, pp. 2020. https://doi.org/10.5067/9831N0JGVAF6. accessed March.
Köhler, P., Guanter, L., Joiner, J., 2015. A linear method for the retrieval of sun-induced chlorophyll fluorescence from GOME-2 and SCIAMACHY data. Atmos. Measur. Techniq. 8, 2589–2608.
Köhler, P., Frankenberg, C., Magney, T.S., Guanter, L., Joiner, J., Landgraf, J., 2018. Global retrievals of solar-induced chlorophyll fluorescence with TROPOMI: first results and Intersensor comparison to OCO-2. Geophys. Res. Lett. 45, 10,456–410,463.
Koster, R.D., Suarez, M.J., Ducharne, A., Stieglitz, M., Kumar, P., 2000. A catchment-based approach to modeling land surface processes in a general circulation model: 1. Model structure. J. Geophys. Res.-Atmos. 105, 24809–24822.
Kumar, S.V., Dirmeyer, P.A., Peters-Lidard, C.D., Bindlish, R., Bolten, J., 2018. Information theoretic evaluation of satellite soil moisture retrievals. Remote Sens. Environ. 204, 392–400.
Li, X., Xiao, J., 2019a. A global, 0.05-degree product of solar-induced chlorophyll fluorescence Derived from OCO-2, MODIS, and reanalysis data. Remote Sens. 11, 517.
Li, X., Xiao, J., 2019b. Mapping photosynthesis solely from solar-induced chlorophyll fluorescence: a global, fine-resolution dataset of gross primary production Derived from OCO-2. Remote Sens. 11, 2563.
Li, X., Xiao, J., 2020. Global climatic controls on interannual variability of ecosystem productivity: similarities and differences inferred from solar-induced chlorophyll fluorescence and enhanced vegetation index. Agric. For. Meteorol. 288-289, 108018.
Li, T., Angeles, O., Radanielson, A., Marcaida, M., Manalo, E., 2015. Drought stress impacts of climate change on rainfed rice in South Asia. Clim. Chang. 133, 709–720.
Li, X., Xiao, J., He, B., 2018b. Higher absorbed solar radiation partly offset the negative effects of water stress on the photosynthesis of Amazon forests during the 2015 drought. Environ. Res. Lett. 13, 044005.
Li, X., Xiao, J., He, B., 2018a. Chlorophyll fluorescence observed by OCO-2 is strongly related to gross primary productivity estimated from flux towers in temperate forests. Remote Sens. Environ. 204, 659–671.
Li, X., Xiao, J., He, B., Arain, M.A., Beringer, J., Desai, A.R., Emmel, C., Hollinger, D.Y., Krasnova, A., Mammarella, I., 2018c. Solar-induced chlorophyll fluorescence is strongly correlated with terrestrial photosynthesis for a wide variety of biomes: first global analysis based on OCO-2 and flux tower observations. Glob. Chang. Biol. 24, 3990–4008.
Li, C., Sun, G., Cohen, E., Zhang, Y., Xiao, J., McNulty, S.G., Meentemeyer, R.K., 2020. Modeling the impacts of urbanization on watershed-scale gross primary productivity and tradeoffs with water yield across the conterminous United States. J. Hydrol. 583, 124581.
Lindsey, R., 2019. Intense Drought in the U.S. Southwest Persisted throughout 2018, Lingers into the New Year. https://www.climate.gov/USdrought2018.
Litvak, M., 2016a. AmeriFlux US-Vcm Valles caldera mixed conifer. In: AmeriFlux. University of New Mexico. https://doi.org/10.17190/AMF/1246121.
Litvak, M., 2016b. AmeriFlux US-Wjs Willard Juniper Savannah. In: AmeriFlux. University of New Mexico. https://doi.org/10.17190/AMF/1246120.
Liu, Z., Kimball, J.S., Parazoo, N.C., Ballantyne, A.P., Wang, W.J., Madani, N., Pan, C.G., Watts, J.D., Reichle, R.H., Sonnentag, O., 2019. Increased high-latitude photosynthetic carbon gain offset by respiration carbon loss during an anomalous warm winter to spring transition. Glob. Chang. Biol. 24, 682–696.
Ma, X., Huete, A., Cleverly, J., Eamus, D., Chevallier, F., Joiner, J., Poulter, B., Zhang, Y., Guanter, L., Meyer, W., 2016. Drought rapidly diminishes the large net CO2 uptake in 2011 over semi-arid Australia. Sci. Rep. 6, 37747.
Madani, N., Kimball, J.S., Jones, L.A., Parazoo, N.C., Guan, K., 2017. Global analysis of bioclimatic controls on ecosystem productivity using satellite observations of solar-induced chlorophyll fluorescence. Remote Sens. 9, 530.
Mishra, A., Vu, T., Veettil, A.V., Entekhabi, D., 2017. Drought monitoring with soil moisture active passive (SMAP) measurements. J. Hydrol. 552, 620–632.
Mladenova, I.E., Bolten, J.D., Crow, W.T., Sazib, N., Cosh, M.H., Tucker, C.J., Reynolds, C., 2019. Evaluating the operational application of SMAP for global agricultural drought monitoring. IEEE J. Select. Topics Appl. Earth Observ. Remote Sens. 12, 3387–3397.
Mohammed, G.H., Colombo, R., Middleton, E.M., Rascher, U., van der Tol, C., Nedbal, L., Goulas, Y., Pérez-Priego, O., Damm, A., Meroni, M., 2019. Remote sensing of solar-induced chlorophyll fluorescence (SIF) in vegetation: 50 years of progress. Remote Sens. Environ. 231, 111177.
Monteith, J.L., Moss, C., 1977. Climate and the efficiency of crop production in Britain [and discussion]. Philos. Transac. Royal Soc. Lond. B 281, 277–294.
Myneni, R.B., Yang, W., Nemani, R.R., Huete, A.R., Dickinson, R.E., Knyazikhin, Y., Didan, K., Fu, R., Juárez, R.I.N., Saatchi, S.S., 2007. Large seasonal swings in leaf area of Amazon rainforests. Proc. Natl. Acad. Sci. 104, 4820–4823.
Nemani, R.R., Keeling, C.D., Hashimoto, H., Jolly, W.M., Piper, S.C., Tucker, C.J., Myneni, R.B., Running, S.W., 2003. Climate-driven increases in global terrestrial net primary production from 1982 to 1999. Science 300, 1560–1563.
NOAA National Centers for Environmental Information, 2018. U.S. Drought Monitor Update for May 1, 2018. https://www.ncei.noaa.gov/news/us-drought-monitor-update-may-1-2018.
Ozelkan, E., Chen, G., Ustundag, B.B., 2016. Multiscale object-based drought monitoring and comparison in rainfed and irrigated agriculture from Landsat 8 OLI imagery. Int. J. Appl. Earth Obs. Geoinf. 44, 159–170.
Parazoo, N.C., Barnes, E., Worden, J., Harper, A.B., Bowman, K.B., Frankenberg, C., Wolf, S., Litvak, M., Keenan, T.F., 2015. Influence of ENSO and the NAO on terrestrial carbon uptake in the Texas-northern Mexico region. Glob. Biogeochem. Cycles 29, 1247–1265.
Potter, C.S., Randerson, J.T., Field, C.B., Matson, P.A., Vitousek, P.M., Mooney, H.A., Klooster, S.A., 1993. Terrestrial ecosystem production: a process model based on global satellite and surface data. Glob. Biogeochem. Cycles 7, 811–841.
Purdy, A.J., Fisher, J.B., Goulden, M.L., Colliander, A., Halverson, G., Tu, K., Famiglietti, J.S., 2018. SMAP soil moisture improves global evapotranspiration. Remote Sens. Environ. 219, 1–14.
Qiu, B., Ge, J., Guo, W., Pitman, A.J., Mu, M., 2020. Responses of Australian Dryland vegetation to the 2019 heat wave at a subdaily scale. Geophys. Res. Lett. 47 (e2019GL086569).
Reichle, R.H., De Lannoy, G.J., Liu, Q., Ardizzone, J.V., Colliander, A., Conaty, A., Crow, W., Jackson, T.J., Jones, L.A., Kimball, J.S., 2017. Assessment of the SMAP level-4 surface and root-zone soil moisture product using in situ measurements. J. Hydrometeorol. 18, 2621–2645.
Reichle, R., De Lannoy, G., Koster, R., Crow, W., Kimball, J., Liu, Q., 2018. SMAP L4 Global 3-Hourly 9 Km EASE-Grid Surface and Root Zone Soil Moisture Analysis Update, Version 4. Boulder, Colorado USA. NASA National Snow and Ice Data Center Distributed Active Archive Center, pp. 2020. https://doi.org/10.5067/60HB8VIP2T8W. accessed March.
Reichle, R.H., Liu, Q., Koster, R.D., Crow, W.T., De Lannoy, G.J., Kimball, J.S., Ardizzone, J.V., Bosch, D., Colliander, A., Cosh, M., 2019. Version 4 of the SMAP Level-4 soil moisture algorithm and data product. J. Adv. Model. Earth Syst. 11, 3106–3130.
Rouse, J.W., Haas, R.H., Schell, J.A., Deering, D.W., 1974. Monitoring vegetation systems. In the Great Plains with ERTS. In: Paper Presented at the 3rd ERTS-1 Symposium. Greenbelt, Maryland.
Running, S.W., Nemani, R.R., Heinsch, F.A., Zhao, M., Reeves, M., Hashimoto, H., 2004. A continuous satellite-derived measure of global terrestrial primary production. Bioscience 54, 547–560.
Ryu, Y., Berry, J.A., Baldocchi, D.D., 2019. What is global photosynthesis? History, uncertainties and opportunities. Remote Sens. Environ. 223, 95–114.
Sadras, V., Grassini, P., Costa, R., Cohan, L., Hall, A., 2014. How reliable are crop production data? Case studies in USA and Argentina. Food Security 6, 447–459.
Samanta, A., Ganguly, S., Hashimoto, H., Devadiga, S., Vermote, E., Knyazikhin, Y., Nemani, R.R., Myneni, R.B., 2010. Amazon forests did not green-up during the 2005 drought. Geophys. Res. Lett. 37.
Scott, R., 2016a. AmeriFlux US-Wkg Walnut Gulch Kendall Grasslands. In: AmeriFlux; United States Department of Agriculture, https://doi.org/10.17190/AMF/1246112.
Scott, R., 2016b. AmeriFlux US-Whs Walnut Gulch Lucky Hills Shrub. In: AmeriFlux; United States Department of Agriculture, https://doi.org/10.17190/AMF/1246113.
Scott, R.L., Huxman, T.E., Cable, W.L., Emmerich, W.E., 2006. Partitioning of evapotranspiration and its relation to carbon dioxide exchange in a Chihuahuan Desert shrubland. Hydrol. Processes 20, 3227–3243.
Scott, R.L., Hamerlynck, E.P., Jenerette, G.D., Moran, M.S., Barron-Gafford, G.A., 2010. Carbon dioxide exchange in a semidesert grassland through drought-induced vegetation change. J. Geophys. Res. Biogeosci. 115.
Smith, W., Biederman, J., Scott, R., Moore, D., He, M., Kimball, J., Yan, D., Hudson, A., Barnes, M., MacBean, N., 2018. Chlorophyll fluorescence better captures seasonal

and interannual gross primary productivity dynamics across dryland ecosystems of southwestern North America. Geophys. Res. Lett. 45, 748–757.
Smith, W.K., Dannenberg, M.P., Yan, D., Herrmann, S., Barnes, M.L., Barron-Gafford, G.A., Biederman, J.A., Ferrenberg, S., Fox, A.M., Hudson, A., 2019. Remote sensing of dryland ecosystem structure and function: Progress, challenges, and opportunities. Remote Sens. Environ. 233, 111401.
Somkuti, P., Bösch, H., Feng, L., Palmer, P.I., Parker, R.J., Quaife, T., 2020. A new space-borne perspective of crop productivity variations over the US Corn Belt. Agric. For. Meteorol. 281, 107826.
Song, L., Guanter, L., Guan, K., You, L., Huete, A., Ju, W., Zhang, Y., 2018. Satellite sun-induced chlorophyll fluorescence detects early response of winter wheat to heat stress in the Indian indo-Gangetic Plains. Glob. Chang. Biol. 24, 4023–4037.
Sun, Y., Fu, R., Dickinson, R., Joiner, J., Frankenberg, C., Gu, L., Xia, Y., Fernando, N., 2015. Drought onset mechanisms revealed by satellite solar-induced chlorophyll fluorescence: insights from two contrasting extreme events. J. Geophys. Res. Biogeosci. 120, 2427–2440.
Sun, Y., Frankenberg, C., Wood, J.D., Schimel, D., Jung, M., Guanter, L., Drewry, D., Verma, M., Porcar-Castell, A., Griffis, T.J., 2017. OCO-2 advances photosynthesis observation from space via solar-induced chlorophyll fluorescence. Science 358, eaam5747.
Svoboda, M., LeComte, D., Hayes, M., Heim, R., Gleason, K., Angel, J., Rippey, B., Tinker, R., Palecki, M., Stooksbury, D., 2002. The drought monitor. Bull. Am. Meteorol. Soc. 83, 1181–1190.
Velpuri, N.M., Senay, G.B., Morisette, J.T., 2016. Evaluating new SMAP soil moisture for drought monitoring in the rangelands of the US high plains. Rangelands 38, 183–190.
Verma, M., Schimel, D., Evans, B., Frankenberg, C., Beringer, J., Drewry, D.T., Magney, T., Marang, I., Hutley, L., Moore, C., 2017. Effect of environmental conditions on the relationship between solar induced fluorescence and gross primary productivity at an OzFlux grassland site. J. Geophys. Res. Biogeosci. 122, 716–733.
Vicente-Serrano, S.M., Gouveia, C., Camarero, J.J., Beguería, S., Trigo, R., López-Moreno, J.I., Azorín-Molina, C., Pasho, E., Lorenzo-Lacruz, J., Revuelto, J., 2013. Response of vegetation to drought time-scales across global land biomes. Proc. Natl. Acad. Sci. 110, 52–57.
Wang, S., Huang, C., Zhang, L., Lin, Y., Cen, Y., Wu, T., 2016. Monitoring and assessing the 2012 drought in the great plains: Analyzing satellite-retrieved solar-induced chlorophyll fluorescence, drought indices, and gross primary production. Remote Sens. 8, 61.
Wang, C., Guan, K., Peng, B., Chen, M., Jiang, C., Zeng, Y., Wu, G., Wang, S., Wu, J., Yang, X., 2020. Satellite footprint data from OCO-2 and TROPOMI reveal significant spatio-temporal and inter-vegetation type variabilities of solar-induced fluorescence yield in the US Midwest. Remote Sens. Environ. 241, 111728.
Wieneke, S., Burkart, A., Cendrero-Mateo, M., Julitta, T., Rossini, M., Schickling, A., Schmidt, M., Rascher, U., 2018. Linking photosynthesis and sun-induced fluorescence at sub-daily to seasonal scales. Remote Sens. Environ. 219, 247–258.
Williams, E., Funk, C., Shukla, S., McEvoy, D., 2020. Quantifying human-induced temperature impacts on the 2018 United States four corners hydrologic and agro-pastoral drought. Bull. Am. Meteorol. Soc. 101, S11–S16.
Wohlfahrt, G., Gerdel, K., Migliavacca, M., Rotenberg, E., Tatarinov, F., Müller, J., Hammerle, A., Julitta, T., Spielmann, F., Yakir, D., 2018. Sun-induced fluorescence and gross primary productivity during a heat wave. Sci. Rep. 8, 1–9.
Wood, J.D., Griffis, T.J., Baker, J.M., Frankenberg, C., Verma, M., Yuen, K., 2017. Multiscale analyses of solar-induced florescence and gross primary production. Geophys. Res. Lett. 44, 533–541.
Wutzler, T., Lucas-Moffat, A., Migliavacca, M., Knauer, J., Sickel, K., Šigut, L., Menzer, O., Reichstein, M., 2018. Basic and extensible post-processing of eddy covariance flux data with REddyProc. Biogeosciences 15, 5015–5030.
Xiao, J., Zhuang, Q., Liang, E., Shao, X., McGuire, A.D., Moody, A., Kicklighter, D.W., Melillo, J.M., 2009. Twentieth-century droughts and their impacts on terrestrial carbon cycling in China. Earth Interact. 13, 1–31.
Xiao, J., Chevallier, F., Gomez, C., Guanter, L., Hicke, J.A., Huete, A.R., Ichii, K., Ni, W., Pang, Y., Rahman, A.F., 2019. Remote sensing of the terrestrial carbon cycle: a review of advances over 50 years. Remote Sens. Environ. 233, 111383.
Yang, X., Tang, J., Mustard, J.F., Lee, J.E., Rossini, M., Joiner, J., Munger, J.W., Kornfeld, A., Richardson, A.D., 2015. Solar-induced chlorophyll fluorescence that correlates with canopy photosynthesis on diurnal and seasonal scales in a temperate deciduous forest. Geophys. Res. Lett. 42, 2977–2987.
Yang, K., Ryu, Y., Dechant, B., Berry, J.A., Hwang, Y., Jiang, C., Kang, M., Kim, J., Kimm, H., Kornfeld, A., 2018. Sun-induced chlorophyll fluorescence is more strongly related to absorbed light than to photosynthesis at half-hourly resolution in a rice paddy. Remote Sens. Environ. 216, 658–673.
Yoshida, Y., Joiner, J., Tucker, C., Berry, J., Lee, J.-E., Walker, G., Reichle, R., Koster, R., Lyapustin, A., Wang, Y., 2015. The 2010 Russian drought impact on satellite measurements of solar-induced chlorophyll fluorescence: insights from modeling and comparisons with parameters derived from satellite reflectances. Remote Sens. Environ. 166, 163–177.
Yu, L., Wen, J., Chang, C., Frankenberg, C., Sun, Y., 2019. High-resolution global contiguous SIF of OCO-2. Geophys. Res. Lett. 46, 1449–1458.
Zeng, Y., Badgley, G., Dechant, B., Ryu, Y., Chen, M., Berry, J.A., 2019. A practical approach for estimating the escape ratio of near-infrared solar-induced chlorophyll fluorescence. Remote Sens. Environ. 232, 111209.
Zhang, Y., Guanter, L., Berry, J.A., van der Tol, C., Yang, X., Tang, J., Zhang, F., 2016. Model-based analysis of the relationship between sun-induced chlorophyll fluorescence and gross primary production for remote sensing applications. Remote Sens. Environ. 187, 145–155.
Zhang, Y., Guanter, L., Joiner, J., Song, L., Guan, K., 2018. Spatially-explicit monitoring of crop photosynthetic capacity through the use of space-based chlorophyll fluorescence data. Remote Sens. Environ. 210, 362–374.
Zhang, Y., Joiner, J., Alemohammad, S.H., Zhou, S., Gentine, P., 2018a. A global spatially contiguous solar-induced fluorescence (CSIF) dataset using neural networks. Biogeosciences 15.
Zhang, Y., Joiner, J., Gentine, P., Zhou, S., 2018b. Reduced solar-induced chlorophyll fluorescence from GOME-2 during Amazon drought caused by dataset artifacts. Glob. Chang. Biol. 24, 2229–2230.
Zhang, Z., Chen, J.M., Guanter, L., He, L., Zhang, Y., 2019. From canopy-leaving to total canopy far-red fluorescence emission for remote sensing of photosynthesis: first results from TROPOMI. Geophys. Res. Lett. 46, 12030–12040.
Zhao, M., Running, S.W., 2010. Drought-induced reduction in global terrestrial net primary production from 2000 through 2009. Science 329, 940–943.
Zhao, M., Heinsch, F.A., Nemani, R.R., Running, S.W., 2005. Improvements of the MODIS terrestrial gross and net primary production global data set. Remote Sens. Environ. 95, 164–176.
Zuromski, L.M., Bowling, D.R., Köhler, P., Frankenberg, C., Goulden, M.L., Blanken, P.D., Lin, J.C., 2018. Solar-induced fluorescence detects interannual variation in gross primary production of coniferous forests in the Western United States. Geophys. Res. Lett. 45, 7184–7193.